Isomeric Equilibria, Nuclear Quantum Effects, and Vibrational Spectra of $M^+(H_2O)_{n=1-3}$ Clusters, with M = Li, Na, K, Rb, and Cs, Through Many-Body Representations

Marc Riera,[†] Sandra E. Brown,[†] and Francesco Paesani[*,‡,¶,§]

†*Department of Chemistry and Biochemistry, University of California, San Diego, La Jolla, California 92093, United States*

‡*Department of Chemistry and Biochemistry, University of California San Diego, La Jolla, California 92093, United States*

¶*Materials Science and Engineering, University of California San Diego, La Jolla, California 92093, United States*

§*San Diego Supercomputer Center, University of California San Diego, La Jolla, California 92093, United States*

E-mail: fpaesani@ucsd.edu

Abstract

A quantitative characterization of the molecular mechanisms that regulate ion solvation is key to the microscopic understanding of fundamental processes taking place in aqueous environments, with major implications for different fields, from atmospheric chemistry to materials research and biochemistry. This study presents a systematic analysis of isomeric equilibria for small $M^+(H_2O)_n$ clusters, with M = Li, Na, K, Rb, and Cs, from 0 K to 200 K. To determine the relative stability of different isomers of

each $M^+(H_2O)_n$ cluster as a function of temperature, replica exchange simulations are carried out at both classical and quantum levels with the recently developed many-body MB-nrg potential energy functions, which have been shown to exhibit chemical accuracy. Anharmonic vibrational spectra are then calculated within the local monomer approximation and found to be in agreement with the available experimental data, providing further support for the accuracy of the MB-nrg potential energy functions. The present analysis indicates that nuclear quantum effects become increasingly important for larger $M^+(H_2O)_n$ clusters containing the heavier alkali metal ions, which is explained in terms of competing ion-water and water-water interactions along with the interplay between energetic and entropic effects. Directly connecting experimental measurements with molecular properties calculated at the quantum mechanical level, this study represents a further step toward the development of a consistent picture of ion hydration from the gas to the condensed phase.

Introduction

Determining the driving forces and molecular mechanisms that regulate ion hydration is key to the microscopic understanding of fundamental processes that take place in aqueous clusters, solutions, and interfaces. For example, charged species are often found as intermediates in chemical reactions and catalytic processes.[1,2] In biochemistry, ions play a central role in the stabilization of biomolecules[3–5] as well as in mediating protein-protein interactions,[6,7] intracellular signal transduction,[8,9] and enzyme and nucleic acid catalysis.[10–13] Ionic clusters carry electric currents and are involved in the formation and evolution of aerosol particles in the atmosphere,[14,15] while ionic solutions are central to many devices such as electrolytic cells, capacitors, and batteries.[16]

The stabilization of individual ions in solution results from the interplay of energetic contributions associated with ion-solvent and ion-ion interactions, and entropic contributions associated with solvent reorganization required to accommodate the charged species. Given

the central role played by electrolyte solutions in different fields of science and engineering, it is not surprising that much experimental and theoretical work has been and continues to be devoted to the development of a molecular-level understanding of ion hydration.[17–20] Although the presence of ions is expected to induce changes in the properties of the water hydrogen-bond (HB) network, the precise determination of the extent to which these changes affect structural, thermodynamic, and dynamical properties of aqueous clusters and solutions remains elusive.[21]

A quantitative description of ion hydration is tightly connected to the ability of accurately representing both water-water and ion-water interactions. In this context, computer simulations that rely either on (empirical) force fields (FFs)[17,22–28] or *ab initio*[17,20,29] models based on density functional theory (DFT) provide a promising route for investigating structural, thermodynamic, and dynamical properties of hydrated ions. Several FFs describing the interactions of various ions with water have been reported in the literature and used, with different degrees of success, in molecular dynamics (MD) simulations of ions in water.[23,26,27,30–38] Most of these FFs treat the water molecules as rigid, which precludes comparisons with experimental vibrational spectra that directly probe the local hydration structure of ions from small gas-phase clusters to solutions.[39–42] On the other hand, while DFT models should, in principle, provide a parameter-free description of all molecular properties, intrinsic limitations in existing exchange-correlation functionals effectively prevent from achieving chemical and spectroscopic accuracy in *ab initio* MD simulations of ions in water.[43]

The prospect for realistic computer simulations of aqueous systems has gained renewed hope[44] with the advent of accurate potential energy functions (PEFs) for water, such as CC-pol,[45–47] WHBB,[48–50] HBB2-pol,[51,52] and MB-pol,[53–55] rigorously derived from the many-body expansion (MBE) of the underlying interaction energies.[56] Not relying on empirical parameterizations, these many-body PEFs allow for actual "predictions" rather than "reproductions" of experimentally measurable quantities.[57] Among existing many-body PEFs,

MB-pol has been shown to correctly predict the vibration-rotation tunneling spectrum of the water dimer,[58] the energetics, quantum equilibria, and infrared spectra of small clusters,[54,59–61] the structural, thermodynamic, and dynamical properties of liquid water,[55,62] the energetics of different ice phases,[63] infrared and Raman spectra of liquid water,[64–66] the sum-frequency generation spectrum of the air/water interface at ambient conditions,[67] the infrared and Raman spectra of ice I_h,[68] and the electronic band gap of liquid water, both in the bulk and at the air/water interface.[69]

Building upon the accuracy of MB-pol for water, many-body PEFs (called MB-nrg for "many-body energy") have recently been introduced to describe halide-water and alkali metal ion-water interactions.[70,71] Derived entirely from electronic structure data obtained at the coupled cluster level with single, double, and perturbative triple excitations, i.e., CCSD(T), the current gold standard for chemical accuracy, these MB-nrg PEFs have been shown to outperform both more advanced, polarizable FFs and existing DFT models in the description of the lower-order, two-body (2B) contributions to the corresponding interaction energies.[70,71] When employed in full-dimensional quantum calculations for $X^-(H_2O)$ and $X^-(D_2O)$ dimers, with X = F, Cl, Br, and I, the MB-nrg PEFs predict vibrational spectra in close agreement with the available experimental data, correctly reproducing anharmonic, nuclear quantum effects, and tunneling splittings.[72]

Along the path connecting ion-water dimers to electrolyte solutions, ion-water clusters in the gas phase play an important role for understanding ion hydration since, due to their relatively small sizes, they are still amenable to high-level electronic structure calculations while, at the same time, they can be studied experimentally using high-resolution vibrational spectroscopy.[73,74] Continuing our systematic efforts aimed at developing an accurate, molecular-level description of hydration phenomena in different environments and under different thermodynamic conditions, in this study, we investigate the structure, and the temperature-dependent isomeric equilibria and vibrational spectra of $M^+(H_2O)_n$ clusters with M = Li, Na, K, Rb, and Cs, and n = 1-3, at both classical and quantum levels using

the MB-nrg PEFs of Ref. 71. The hydration of alkali metal ions has been extensively studied both experimentally[75] and theoretically.[76–78] However, there is not yet a clear consensus between theory and experiments on the hydration structure of these ions in solution.[79] Particularly relevant to our analysis are the infrared photodissociation spectra reported in Refs. 39,41,80–82 and the theoretical studies of Refs. 79,83–86.

Computational Details

Following the same theoretical/computational approach used for neutral water clusters,[53,61,87] thermodynamic equilibria between different isomers of $M^+(H_2O)_n$ clusters, with $n = 2$ and 3, and M = Li, Na, K, Rb, and Cs, were characterized at both classical and quantum levels using replica exchange molecular dynamics (REMD) and replica exchange path-integral molecular dynamics (REPIMD), respectively. Both REMD and REPIMD simulations were carried out with the MB-nrg PEFs introduced in Ref. 71 using 64 replicas between 10 K and 200 K, except for $Li^+(H_2O)_2$ for which the temperatures ranged from 10 K to 250 K, and for $Li^+(H_2O)_3$ and $Na^+(H_2O)_3$ for which the temperatures ranged from 10 K to 350 K. In both REMD and REPIMD simulations, the replicas were distributed according to a geometric temperature progression, which helps ensure efficient exchange between different replicas at both low and high temperature.

In the REPIMD simulations, which provide numerically exact, quantum equilibrium distributions of the different isomers of each $M^+(H_2O)_n$ cluster, each atom was represented by a Feynman's ring polymer with P = 64 beads.[88] After 1 ns of equilibration, classical and quantum equilibrium distributions of the different isomers were obtained from 9 ns of REMD and 3 ns of REPIMD simulations, respectively, with a timestep of 0.2 fs. Instantaneous configurations for the $M^+(H_2O)_n$ clusters were extracted every 2 ps from each replica along the REMD simulations and quenched to identify possible isomers through geometry optimizations carried out by combining linear search and conjugate gradient methods, with

a threshold of 10^{-8} kcal mol^{-1}Å^{-1} for the gradients.[89]

To characterize how the presence of different alkali metal ions affect the spatial arrangements and HB network of the solvating water molecules, (anharmonic) infrared spectra of all isomers were calculated by combining the local-mode[90,91] and local-monomer[49] (LM) methods as described in Ref. 61. By neglecting intermonomer, two-mode and higher-order anharmonic couplings, the LM method provides an approximate, yet accurate, solution to the vibrational Schrödinger equation.[91] For reference, harmonic spectra were also calculated to quantify the importance of nuclear quantum effects and anharmonicity (see Supporting Information). Harmonic frequencies obtained for both symmetric and asymmetric stretches of the water molecules were found to be blueshifted by $\sim$190 cm^{-1} and 150 cm^{-1} relative to the corresponding LM values, respectively. These differences suggest that some caution should be used in comparing vibrational spectra obtained from classical MD simulations of ions in aqueous clusters and solutions with the corresponding experimental data, since, neglecting nuclear quantum effects, MD simulations significantly underestimate the anharmonicity of the underlying Born-Oppenheimer potential energy surface and, therefore, effectively provide harmonic vibrational spectra. Temperature dependent IR spectra of each $M^+(H_2O)_n$ cluster were calculated as weighted combinations of the individual IR spectra of the different isomers, with weights corresponding to the isomer fractions as predicted by the REPIMD simulations. It should be noted that, by construction, these temperature-dependent IR spectra are thus approximations to the actual spectra, neglecting both homogeneous and inhomogeneous broadening, and dynamical effects.

Results

Low-lying isomers of all $M^+(H_2O)_n$ clusters with $n = 1 - 3$ are shown in Figure 1. Each isomer is labeled with the acronym M$l(n)$, where M = L, N, K, R, and C correspond to Li^+, Na^+, K^+, Rb^+ and Cs^+, respectively, l indicates the rank in increasing binding energy (i.e.,

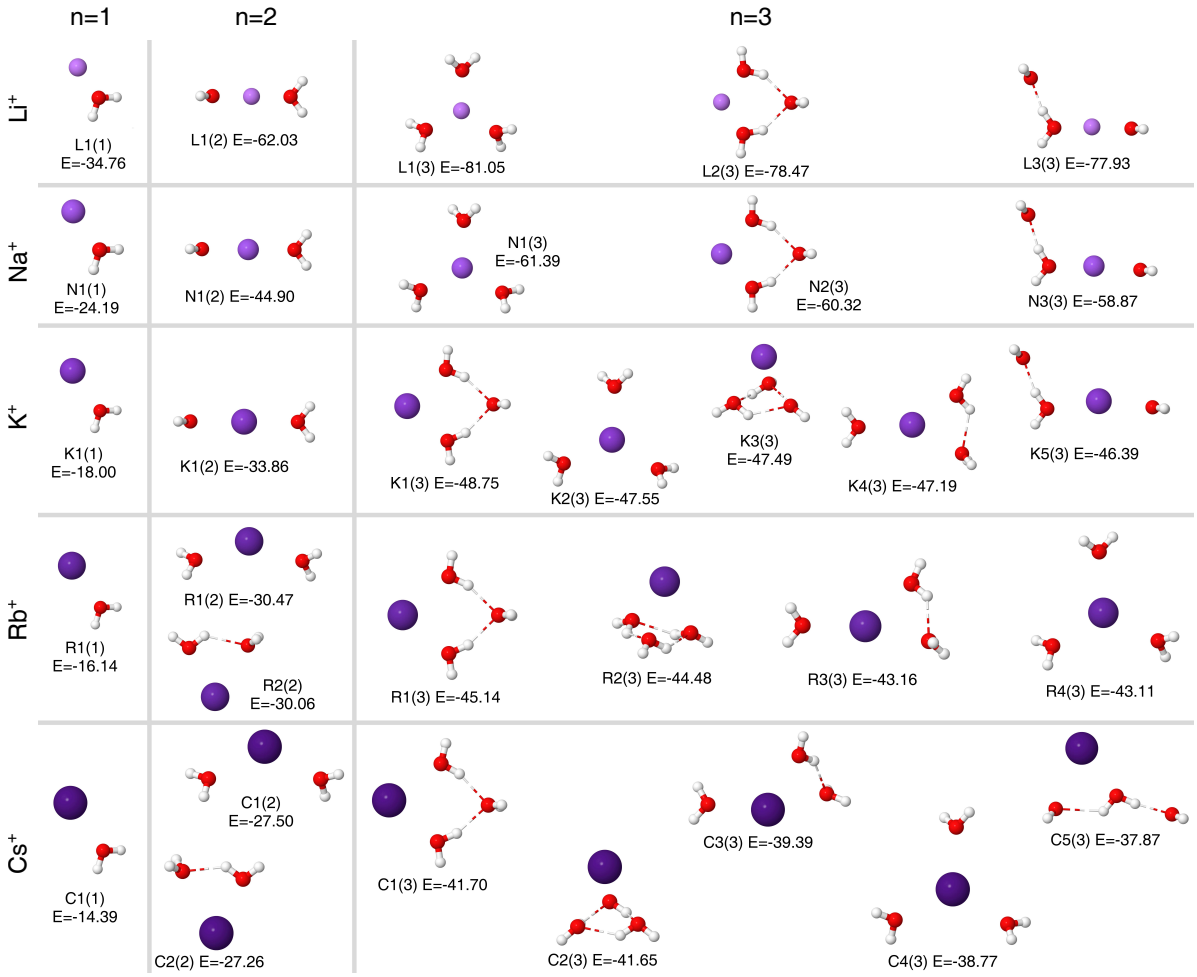

Figure 1: Low-lying isomers of all $M^+(H_2O)_n$ clusters with $n = 1-3$. Each isomer is labeled with the acronym M$l(n)$, where M = L, N, K, R, and C, corresponding to Li^+, Na^+, K^+, Rb^+ and Cs^+, respectively, l indicates the rank in increasing binding energy (i.e., $l = 1$ indicates the minimum-energy structure), and n is the number of water molecules in the cluster. For each isomer, the MB-nrg binding energy (E) is reported in units of kcal/mol.

$l = 1$ indicates the minimum-energy structure), and n is the number of water molecules in the cluster.

$M^+(H_2O)$ clusters

Given both anisotropy and strength of alkali metal ion - water interactions, only one low-lying isomer was identified for each $M^+(H_2O)$ dimer. Since these dimers have been characterized in Ref. 71 through extensive comparisons of MB-nrg with CCSD(T) and DFT calculations,

Table 1: LM anharmonic frequencies (in cm^{-1}) calculated with the MB-nrg PEFs for $M^+(H_2O)$ dimers, with M = Li, Na, K, Rb, Cs, compared with the corresponding values calculated for an isolated H_2O molecule. In parentheses are the available experimental values, with the superscripts indicating the reference numbers.

	H_2O	$Li^+(H_2O)$	$Na^+(H_2O)$	$K^+(H_2O)$	$Rb^+(H_2O)$	$Cs^+(H_2O)$
Bend	1582.0 (1595) [92]	1632.6 –	1630.6 –	1625.9 –	1623.3 –	1620.3 –
Symmetric stretch	3656.0 (3657.0) [93]	3628.7 (3631.0) [41]	3642.4 (3634.5) [41]	3636.5 (3636.0) [41]	3636.5 (3637.0) [82]	3634.7 (3635.4) [41]
Asymmetric stretch	3741.4 (3756.0) [93]	3655.8 (3696.0) [41]	3690.6 (3707.0) [41]	3688.2 (3710.0) [41]	3692.0 (3600-3800) [82]	3691.5 (3711.5) [41]

we will briefly summarize here their main features that will serve as a reference for analyzing the evolution of the hydration properties in larger clusters. Figure 1 shows that, independent of the specific ion, all dimers display similar structures, with the ion being located along the HOH bisector but on the opposite side of the hydrogen atoms. The different chemical nature (e.g., size) and electronic properties (e.g., charge density) of each alkali metal ion directly correlate with the variation of the dimer binding energies, which decrease by ∼20 kcal/mol from $Li^+(H_2O)$ to $Cs^+(H_2O)$.

From the analysis of the vibrational frequencies listed in Table 1, it is clear that the different strength of the interaction between a water molecule and each of the five alkali metal ions translates into different frequency shifts for the water bending and (symmetric and asymmetric) stretching modes, with Li^+ and Cs^+ providing the largest and smallest shifts, respectively. This can be explained by considering that, due to its higher charge density, Li^+ is more effective in drawing electrons from the water molecule which, in turns, weakens the OH bonds and thus shifts the bending and (symmetric and asymmetric) stretching frequencies more to the blue and the red, respectively, compared to the other M^+ ions. In all cases, the LM vibrational frequencies are in good agreement with the available experimental values,[80–82] with deviation ranging from 20 to 30 cm^{-1}, depending on the ion. These differences may be due to a combination of different factors. First, as mentioned above, the LM method neglects intermonomer, two-mode and higher-order anharmonic couplings, which im-

plies that it only provides an approximate solution to the vibrational Schrödinger equation. In this regard, it should be noted that the LM vibrational frequencies reported in Table 1 for a single water molecule differ by ∼30 cm^{-1} from the corresponding values obtained from fully coupled quantum calculations in Ref. 94 using the same potential energy surface. Second, the experimental frequencies were obtained from argon-tagging predissociation spectra measured at low, but undetermined, temperature. Besides possible thermal effects that are not considered in the calculations, which strictly correspond to a temperature of 0 K, the effects of Ar-tagging are difficult to quantify. While the interaction between the argon atom and the $M^+(H_2O)$ dimer is supposed to be relatively small for water complexes containing the heavier alkali metal ions, it represents a large fraction of the total interaction energy of the complex with Li^+ and Na^+. Finally, although the MB-nrg PEFs provides an accurate representation of the underlying M^+–H_2O multidimensional potential energy surfaces, they are associated with root-mean-square-deviations (RMSDs) on the order of 0.05 kcal/mol from CCSD(T) reference values, which translates in blueshifts of ∼20 cm^{-1} for the water vibrations relative to the corresponding CCSD(T) values.[71]

$M^+(H_2O)_2$ clusters

As shown in Figure 1, the addition of a second water molecule leads to some diversification among $M^+(H_2O)_2$ clusters with different M^+ ions. Specifically, while Li^+, Na^+, and K^+ form only one low-lying, linear isomer, with the two water molecules being coordinate through the oxygen atom at opposite sides of the ion, a second, cyclic isomer exists for both $Rb^+(H_2O)_2$ and $Cs^+(H_2O)_2$, in which the two water molecules are hydrogen bonded to each other. As a result, the vibrational spectra of $M^+(H_2O)_2$ clusters with M = Li, Na, and K at 0 K show the same features as those of the corresponding dimers, with the symmetric stretch at ∼3640 cm^{-1} and the asymmetric stretch at ∼3700 cm^{-1}. Since only one low-lying isomer exists for these complexes, the IR spectra are predicted to remain effectively unchanged in the temperature range from 0 K to 200 K examined in this study. In addition, due to the

Table 2: Relative ZPE-corrected binding energies (in kcal/mol) calculated for $M^+(H_2O)_2$ clusters, with M = Li, Na, K, Rb, and Cs, using the MB-nrg PEF. The corresponding binding energies on the underlying Born-Oppenheimer potential energy surface are shown in Figure 1.

Isomer	$Li^+(H_2O)_2$	$Na^+(H_2O)_2$	$K^+(H_2O)_2$	$Rb^+(H_2O)_2$	$Cs^+(H_2O)_2$
1	0.00	0.00	0.00	0.00	0.89
2	–	–	–	1.37	0.00

absence of other isomers, only REMD simulations were carried out for these clusters.

The different chemical and physical properties (e.g., size, charge density, and polarizability) of Rb^+ and Cs^+ result in weaker ion-water interactions that thus enter in competition with the water-water interaction within the $M^+(H_2O)_2$ cluster. As a result, the perfectly linear structure of the only isomer found with Li^+, Na^+, and K^+, becomes increasingly distorted going from Rb^+, with an $\widehat{OM^+O}$ angle of 140.9^o, to Cs^+, with an $\widehat{OM^+O}$ angle of 120.3^o. Importantly, while this nearly linear structure remains the minimum energy isomer for $Rb^+(H_2O)_2$, it becomes the second low-lying isomer for $Cs^+(H_2O)_2$, which clearly demonstrates the increasing relative importance of water-water hydrogen bonding in the stabilization of $M^+(H_2O)_n$ clusters, with $n > 1$.

As shown in Figure 1, the Born-Oppenheimer energy differences between the two lowest isomers of $Rb^+(H_2O)_2$ and $Cs^+(H_2O)_2$ are 0.41 kcal/mol and 0.24 kcal/mol, respectively. However, after inclusion of the corresponding zero-point energies (ZPEs) within the harmonic approximation, Table 2 shows that the C2(2) isomer becomes the actual ground state of $Cs^+(H_2O)_2$, lying 0.89 kcal/mol below C1(2), while R1(2) remains the lowest-lying isomer of $Rb^+(H_2O)_2$, lying 1.37 kcal/mol below R2(2). The different role played by nuclear quantum effects on the relative stability of $Rb^+(H_2O)_2$ and $Cs^+(H_2O)_2$ clusters becomes even more apparent from the analysis of the REMD and REPIMD results shown in Figure 2. While the fractions of R1(2) and R2(2) calculated at both classical and quantum levels are identical at all temperatures, the REMD simulations predict that C1(2) is the most abundant isomer below 10 K before sharply decreasing up to $\sim$40 K and then slowing increasing as the

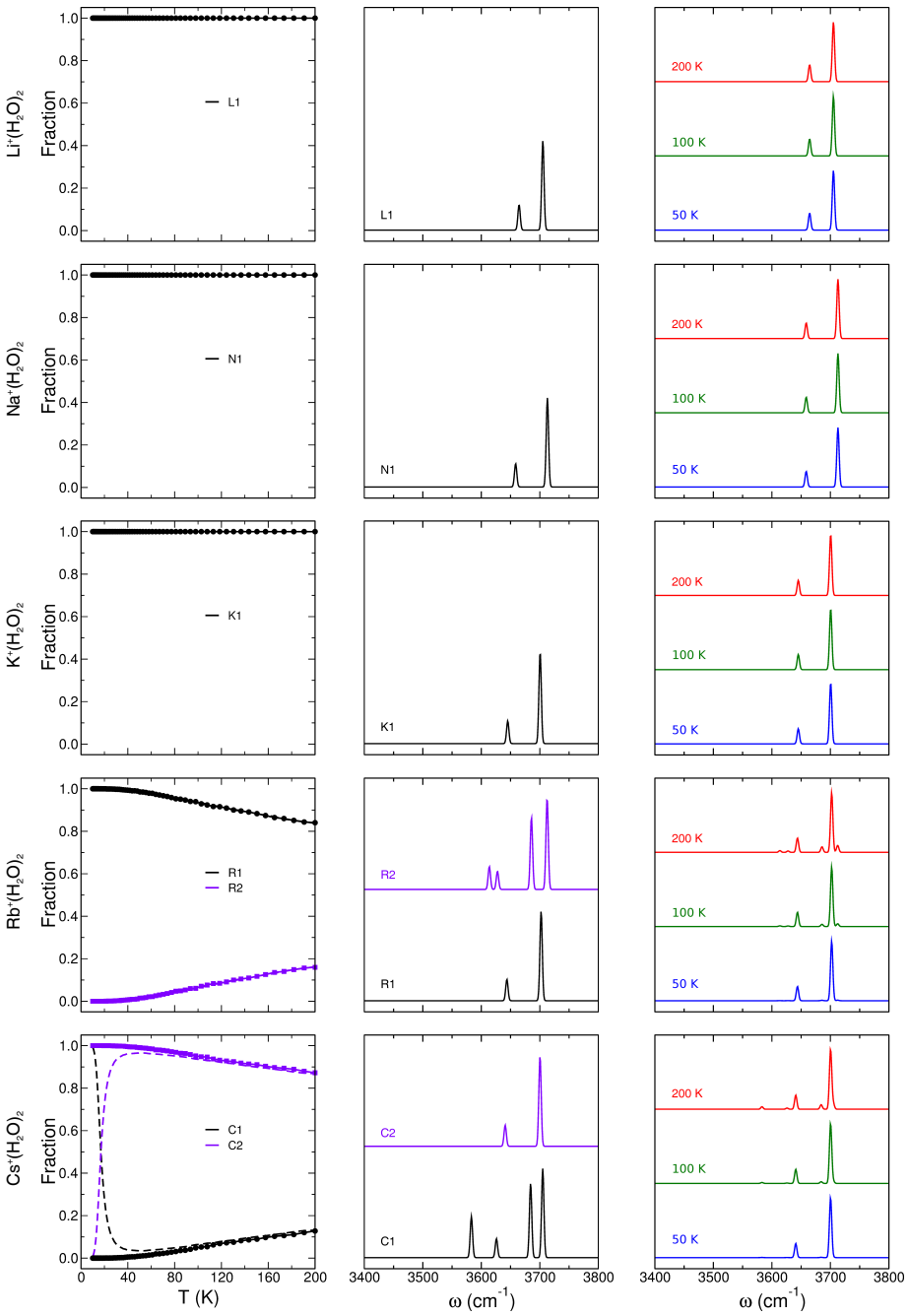

Figure 2: Left column: Fractions of different isomers of each $M^+(H_2O)_2$ cluster, with M = Li, Na, K, Rb, and Cs, calculated using REMD (dashed lines) and REPIMD (solid lines) simulations as a function of temperature. Middle column: LM anharmonic vibrational spectra calculated for individual isomers at 0 K and smoothed using Gaussians with standard deviations of 2 cm^{-1}. Right column: Vibrational spectra calculated for each $M^+(H_2O)_2$ cluster at 50 K, 100 K, and 200 K as weighted combinations of the individual isomer spectra (middle column), with weights corresponding to the isomer fractions as predicted by the REPIMD simulations (left column).

temperature increases. In contrast, by correctly including nuclear quantum effects, the REPIMD simulations show that C2(2) is the most stable isomer over the entire temperature range, from 0 K to 200 K.

Since the nearly linear isomer of both $Rb^+(H_2O)_2$ and $Cs^+(H_2O)_2$ clusters effectively dominates at all temperatures, the corresponding IR spectra are very similar to those calculated for the analogous clusters with Li^+, Na^+, and K^+, displaying two main peaks associated with the symmetric and asymmetric stretches of the water molecules. Minor spectral features associated with "cyclic" isomers appear at temperature higher than 100 K. Overall, the calculated spectra are in agreement with the available experimental data.[41,82] However, it should be noted that the experimental spectra also display minor features above 3750 cm^{-1} corresponding to $\Delta K = \pm 1$ rotational subbands of the water asymmetric stretching mode,[80] which, by construction, cannot be reproduced by the LM method.

$M^+(H_2O)_3$ clusters

The addition of a third water molecule in the hydration shell of M^+ ions gives rise to a more diverse group of low-lying isomers which now includes linear, branched, and cyclic structures, with and without hydrogen-bonded water molecules. As shown in Figure 1, there are significant structural differences between the minimum-energy configurations of $M^+(H_2O)_3$ clusters with $M^+ = Li^+$ and Na^+, and those containing Rb^+ and Cs^+, with the former corresponding to symmetric, branched configurations with the ion in the center of a triangle that has the water molecules at the three vertices, and the latter corresponding to rhombic configurations with the three water molecules and the ion located at the four vertices. Another important structural difference between $M^+(H_2O)_3$ clusters containing the lighter (Li^+ and Na^+) and the heavier (K^+, Rb^+, and Cs^+) ions is the appearance of configurations in which the ion is located on top of planar, hydrogen-bonded triangular structures formed by the three water molecules. Importantly, when ZPE contributions are taken into account within the harmonic approximation, Table 3 shows that the relative

Table 3: Relative ZPE-corrected binding energies (in kcal/mol) calculated for $M^+(H_2O)_3$ clusters, with M = Li, Na, K, Rb, and Cs, using the MB-nrg PEF. The corresponding binding energies on the underlying Born-Oppenheimer potential energy surface are shown in Figure 1.

Isomer	$Li^+(H_2O)_3$	$Na^+(H_2O)_3$	$K^+(H_2O)_3$	$Rb^+(H_2O)_3$	$Cs^+(H_2O)_3$
1	0.00	0.00	0.88	0.15	0.00
2	4.28	2.94	0.00	1.31	0.73
3	3.56	3.18	2.40	0.93	1.21
4	–	–	1.08	0.00	0.64
5	–	–	2.01	–	2.96

stability of the $K^+(H_2O)_3$ and $Rb^+(H_2O)_3$ isomers changes, with the branched configuration becoming the ground state as seen for $Li^+(H_2O)_3$ and $Na^+(H_2O)_3$. The rhombic structure, C1(3), remains the ground state for $Cs^+(H_2O)_3$ upon inclusion of the ZPE, although the branched configuration becomes the second low-lying configuration (see Table 3). These ion-dependent structural differences clearly point to a subtle balance between ion-water and water-water interactions on the underlying Born-Oppenheimer potential energy surface, and nuclear quantum effects.

As shown in Figure 3, while the relative stabilities of the isomers of both $Li^+(H_2O)_3$ and $Na^+(H_2O)_3$ do not change as the temperature increases, with the corresponding minimum-energy structures being the only observed structures below 200 K, the isomeric equilibria for the other $M^+(H_2O)_3$ clusters depend significantly on temperature and display nonnegligible nuclear quantum effects which, depending on M^+, may persist up to temperatures higher than 100 K. For $K^+(H_2O)_3$, isomer K2(3) remains the dominant isomer at the quantum mechanical level, although the fraction of isomer K4(3) increases continuously starting at $\sim$40 K. Importantly, at the classical level, isomer K1(3), corresponding to the minimum-energy structure on the Born-Oppenheimer potential energy surface, disappears quickly between $\sim$10 K and $\sim$40 K, while the fraction of isomer K2(3) steeply increases in the same temperature interval. This inversion in the relative stability of the two lowest-lying isomers can be explained by considering the higher entropy associated with isomer K2(3), in which

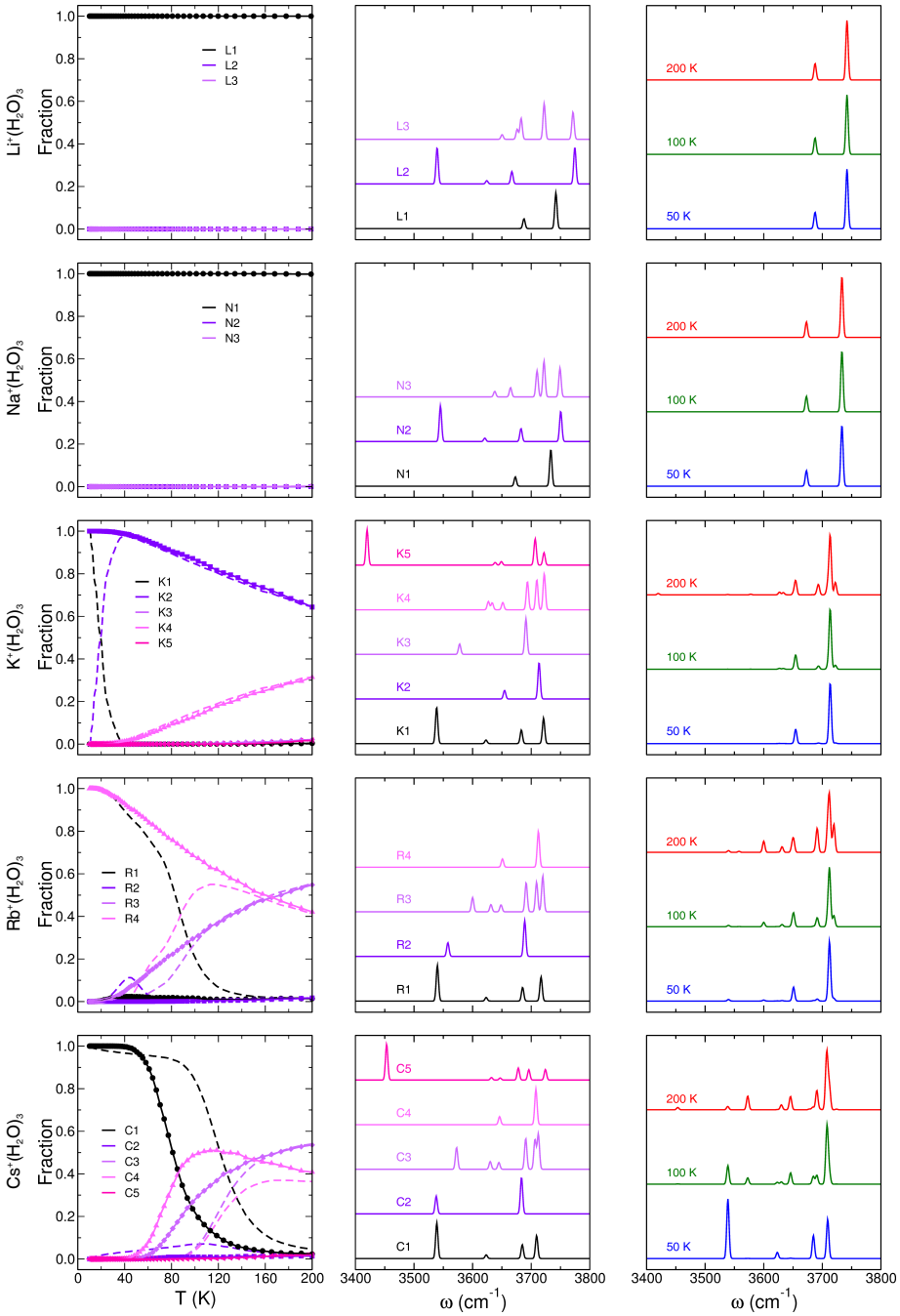

Figure 3: Left column: Fractions of different isomers of each $M^+(H_2O)_3$ cluster, with M = Li, Na, K, Rb, and Cs, calculated using REMD (dashed lines) and REPIMD (solid lines) simulations as a function of temperature. Middle column: LM anharmonic vibrational spectra calculated for individual isomers at 0 K and smoothed using Gaussians with standard deviations of 2 cm^{-1}. Right column: Vibrational spectra calculated for each $M^+(H_2O)_3$ cluster at 50 K, 100 K, and 200 K as weighted combinations of the individual isomer spectra (middle column), with weights corresponding to the isomer fractions as predicted by the REPIMD simulations (left column).

all OH bonds of the three water molecules are free. It should also be noted that the fractions of the different isomers of $K^+(H_2O)_3$ calculated at both classical and quantum levels become effectively indistinguishable above ∼40 K.

Nuclear quantum effects clearly play a major role in determining the relative stability of the different isomers of $Rb^+(H_2O)_3$ and $Cs^+(H_2O)_3$. In particular, the minimum-energy structure, isomer R1(3), of $Rb^+(H_2O)_3$, which is the most abundant isomer at the classical level up to ∼80 K, is not present at any temperature when ZPE contributions are taken into account within the REPIMD formalism. Similarly, the fraction of isomer R2(3), which appears between ∼20 K and ∼40 K in the classical simulations, is negligible over the entire temperature range in the corresponding REPIMD simulations, which instead predict isomers R4(3) and R3(3) to be the most stable structures below and above ∼160 K, respectively. The analysis of the REMD and REPIMD results shows that the crossover from quantum to classical behavior in $Rb^+(H_2O)_3$ also takes place at ∼160 K. While both REMD and REPIMD simulations predict isomer C1(3) to be the most stable structure of $Cs^+(H_2O)_3$ at low temperature, nuclear quantum effects modify the relative stability of the other isomers. Specifically, REPIMD simulations predict isomers C4(3) and C3(3) to become the most stable structures at ∼80 K and ∼150 K, respectively, with negligible fractions of isomers C2(3) and C5(3) present above ∼100 K. In contrast, at the classical level, isomer C1(3) remains the dominant structure up to ∼120 K, after which isomer C3(3) becomes the most stable structure. The REMD simulations also predict isomer C4(3) to represent a relatively large fraction between ∼120 K and ∼200 K, as well as a small, but nonnegligible, fraction of isomer C2(3) over the entire temperature range, and a slowly increasing fraction of isomer C5(3) above ∼100 K. This analysis suggests that, for $Cs^+(H_2O)_3$, the crossover temperature from classical to quantum behavior occurs above 200 K.

Since each $M^+(H_2O)_3$ isomer is characterized by a specific hydrogen-bonding motif, the temperature dependence of the isomeric equilibria is directly mirrored by the evolution of the corresponding infrared spectra. As follows from L1(3) and N1(3) being the only isomers

present in the entire temperature range, the calculated infrared spectra of both $Li^+(H_2O)_3$ and $Na^+(H_2O)_3$ are characterized by two peaks corresponding to the symmetric and anti-symmetric stretches of the three equivalent water molecules of the L1(3) and N1(3) isomers, respectively, which are the only isomers present over the entire temperature range. The LM frequencies, $\sim$3680 cm^{-1} and $\sim$3740 cm^{-1} for $Li^+(H_2O)_3$, and $\sim$3660 cm^{-1} and $\sim$3730 cm^{-1} for $Na^+(H_2O)_3$, are within 20-30 cm^{-1} of the experimental frequencies measured in Ar-tagged predissociation experiments.[41]

Richer infrared spectra are calculated at different temperatures for $M^+(H_2O)_3$ clusters with the heavier ions. Since, at the quantum mechanical level, the dominant isomer of $K^+(H_2O)_3$ is isomer K2(3), which is isostructural with L1(3) and N1(3), the calculated infrared spectra are characterized by analogous symmetric and asymmetric stretch peaks at $\sim$3655 cm^{-1} and $\sim$3710 cm^{-1}, with additional spectral features associated primarily with isomer K4(3) appearing at higher temperature. Overall, good agreement is found with the Ar-tagged predissociation measurements reported in Ref. 41, although the experimental spectra also shown a feature at 3546 cm^{-1}, which is an unambiguous signature of a weak hydrogen bond. The LM spectra calculated for the individual isomers of $K^+(H_2O)_3$ indicates that this spectral feature can be associated with isomer K1(3). Since this isomer is predicted not to be present for the untagged clusters under the equilibrium conditions enforced by the REPIMD formalism, it is possible that it was observed in experiments due to stabilization effects associated with Ar-tagging or because it was trapped under nonequilibrium conditions during the supersonic expansion.

As discussed above, nuclear quantum effects are particularly pronounced in $Rb^+(H_2O)_3$, with two isomers, R3(3) and R4(3), effectively being present with significant fractions at all temperatures. This is mirrored by the corresponding infrared spectra calculated as a function of temperature, which are dominated by isomer R4(3) at low temperature and progressively evolve into combined spectra, with dominant features between 3600 cm^{-1} and 3750 cm^{-1} primarily associated with both R3(3) and R4(3) isomers, and smaller peaks at 3540 cm^{-1} and

3550 cm^{-1} associated with strong hydrogen bonds characteristic of isomers R1(3) and R2(3), respectively. Also for $Rb^+(H_2O)_3$, good agreement is found with the experimental spectra reported in Ref. 95, especially for the frequencies of the water symmetric and asymmetric stretches. However, it should be noted that the experimental intensity of the hydrogen-bond peak at 3550 cm^{-1} is significantly higher than that predicted by the present LM calculations. Such differences between theoretical predictions and experimental measurements, and may be due to the presence of the tagging species in the experiments, inaccuracies in the representation of the many-body dipole moment surface in the calculations, or a combination of the two.

$Cs^+(H_2O)_3$ is the first $M^+(H_2O)_3$ cluster in which the most stable isomer, C1(3), corresponds to a rhombic structure with the ion and the three hydrogen-bonded water molecules at the vertices. As a result, the infrared spectra at low temperature display the characteristic signature of hydrogen bonding at ∼3540 cm^{-1}, which progressively disappears as the temperature increases and isomer C3(3) and C4(3) become increasingly more stable. The LM spectra presented in Figure 3 can be compared with two sets of measurements reported in Refs. 41 and 95. Both measured and calculated spectra display well-defined features at ∼3540 cm^{-1} and ∼3710 cm^{-1} corresponding to water hydrogen-bonded and free OH stretches, respectively. The most recent measurements[95] also show a distinct band at ∼3650 cm^{-1}, which can be assigned to the water symmetric stretches of isomer C4(3), with a small shoulder at ∼3540 cm^{-1}, which correspond to hydrogen-bonded OH stretches of isomer C3(3). While good agreement between measured and calculated spectra is found for all these features, the experimental spectra also show a band at ∼3600 cm^{-1}, which is not present in any of the LM spectra calculated for the individual isomers and, consequently, does not show up in the corresponding temperature-dependent spectra. This discrepancy between experiment measurements and theoretical predictions appears to require further investigation.

Conclusions

We have presented a detailed analysis, at both classical and quantum levels, of the temperature dependence of isomeric equilibria and vibrational spectra of $M^+(H_2O)_n$ clusters, with n = 1 - 3, and $M^+ = Li^+$, Na^+, K^+, Rb^+, and Cs^+, calculated with the MB-nrg PEFs introduced in Ref. 71. Nuclear quantum effects are found to play a negligible role in determining the relative stability of different isomers of clusters containing the lighter ions, Li^+ and Na^+, with one structure of each $M^+(H_2O)_n$ cluster effectively dominating the isomeric equilibria over the temperature range between 0 K and 200 K. Although the low number of water molecules considered in this study is not sufficient to fully complete the first solvation shell around Li^+ and Na^+, the most stable structures of $Li^+(H_2O)_n$ and $Na^+(H_2O)_n$ clusters tend to resemble those found in solution, with the ion at the center of the cluster. At the classical level, competing effects between ion-water and water-water interactions become more pronounced for the heavier ions, which results in a larger number of low-lying isomers, some of which appear to serve initial seeds for extended hydrogen-bonded networks. Within this picture, K^+ holds a special place since, at the classical level, the relative stability of its clusters with water follows a similar trend as that of the lighter ions at low temperature and as that of the heavier ions at high temperature.

When nuclear quantum effects are explicitly taken into account within the path-integral formalism, the relative stability of $K^+(H_2O)_n$ clusters is largely modified by zero point energy contributions which shift the isomeric equilibria toward structures with no hydrogen-bonded water molecules, such as those predicted for $Li^+(H_2O)_n$ and $Na^+(H_2O)_n$ clusters. Similar trend is followed by $Rb^+(H_2O)_n$ clusters, which, however, exhibit increasing stability for isomers containing hydrogen-bonded water molecules. Water clusters containing Cs^+ are the first ones for which the most stable structures correspond to isomers where the ion is interacting with a network of two and three hydrogen-bonded water molecules.

For all clusters, good agreement is found between anharmonic vibrational spectra calculated within the local monomer approximation and the available experimental data.[41,80–82]

Besides providing further support for the accuracy of the MB-nrg PEFs, this level of agreement emphasizes the importance of taking properly into account anharmonic and quantum effects in computer simulations for a correct description of $M^+(H_2O)_n$ clusters. Importantly, the possibility to directly connect experimental measurements with computer simulations at the molecular level provides hope for the development of a consistent picture of ion hydration from the gas to the condensed phase.

Supplementary Material

Geometries for all isomers of each $M^+(H_2O)_n$ cluster, along with the corresponding REMD and REPIMD fractions, and harmonic and anharmonic vibrational spectra calculated at 0 K, along with their corresponding intensities.

Acknowledgements

We thank Pushp Bajaj and Dr. Andreas Götz for valuable discussions. This research was supported by the National Science Foundation through grant CHE-1453204 and used resources of the Extreme Science and Engineering Discovery Environment (XSEDE),[96] which is supported by the National Science Foundation through grant ACI-1053575, under allocation TG-CHE110009 on Comet at the San Diego Supercomputer Center and Stampede2 at the Texas Advanced Computing Center. M.R.R. was supported by a Software Fellowship from the Molecular Sciences Software Institute, which is funded by the National Science Foundation through grant ACI-1547580.

References

(1) Sneen, R. A. Substitution at a Saturated Carbon Atom. XVII. Organic Ion Pairs as Intermediates in Nucleophilic Substitution and Elimination Reactions. *Acc. Chem. Res.*

1973, *6*, 46–53.

(2) Pregel, M.; Dunn, E.; Nagelkerke, R.; Thatcher, G.; Buncel, E. Alkali–Metal lon Catalysis and Inhibition in Nucleophilic Displacement Reaction of Phosphorus–Sulfur–and Carbon– Based Esters. *Chem. Soc. Rev.* **1995**, *24*, 449–455.

(3) Nahar, S.; Tajmir-Riahi, H. Do Metal Ions Alter the Protein Secondary Structure of a Light-Harvesting Complex of Thylakoid Membranes? *J. Inorg. Biochem.* **1995**, *58*, 223–234.

(4) Woodson, S. A. Metal Ions and RNA Folding: A Highly Charged Topic with a Dynamic Future. *Curr. Opin. Chem. Biol.* **2005**, *9*, 104–109.

(5) Draper, D. E. RNA Folding: Thermodynamic and Molecular Descriptions of the Roles of Ions. *Biophys. J.* **2008**, *95*, 5489–5495.

(6) Siuzdak, G.; Ichikawa, Y.; Caulfield, T. J.; Munoz, B.; Wong, C. H.; Nicolaou, K. Evidence of Calcium^{2+}-Dependent Carbohydrate Association Through Ion Spray Mass Spectrometry. *J. Am. Chem. Soc.* **1993**, *115*, 2877–2881.

(7) Tan, Z.-J.; Chen, S.-J. Ion-Mediated Nucleic Acid Helix-Helix Interactions. *Biophys. J.* **2006**, *91*, 518–536.

(8) Endo, M. Calcium Ion as a Second Messenger with Special Reference to Excitation-Contraction Coupling. *J. Pharm. Sci.* **2006**, *100*, 519–524.

(9) Orlov, S.; Hamet, P. Intracellular Monovalent Ions as Second Messengers. *J. Memb. Biol.* **2006**, *210*, 161–172.

(10) Sträter, N.; Lipscomb, W. N.; Klabunde, T.; Krebs, B. Two-Metal Ion Catalysis in Enzymatic Acyl-and Phosphoryl-Transfer Reactions. *Angew. Chem. Int. Ed.* **1996**, *35*, 2024–2055.

(11) Sigel, R. K.; Pyle, A. M. Alternative Roles for Metal Ions in Enzyme Catalysis and the Implications for Ribozyme Chemistry. *Chem. Rev.* **2007**, *107*, 97–113.

(12) Hanna, R.; Doudna, J. A. Metal Ions in Ribozyme Folding and Catalysis. *Curr. Opin. Chem. Biol.* **2000**, *4*, 166–170.

(13) Stahley, M. R.; Strobel, S. A. RNA Splicing: Group I Intron Crystal Structures Reveal the Basis of Splice Site Selection and Metal Ion Catalysis. *Curr. Opin. Struct. Biol.* **2006**, *16*, 319–326.

(14) Harrison, R. G.; Tammet, H. Ions in the Terrestrial Atmosphere and Other Solar System Atmospheres. *Space Sci. Rev.* **2008**, *137*, 107–118.

(15) Lehtipalo, K. et al. The effect of Acid–Base Clustering and Ions on the Growth of Atmospheric Nano-Particles. *Nat. Commun.* **2016**, *7*, 11594.

(16) Winter, M.; Brodd, R. J. What Are Batteries, Fuel Cells, and Supercapacitors? *Chem. Rev.* **2004**, *104*, 4245–4270.

(17) Jungwirth, P.; Tobias, D. J. Specific Ion Effects at the Air/Water Interface. *Chem. Rev.* **2006**, *106*, 1259–1281.

(18) Bakker, H. Structural Dynamics of Aqueous Salt Solutions. *Chem. Rev.* **2008**, *108*, 1456–1473.

(19) Marcus, Y. Effect of Ions on the Structure of Water: Structure Making and Breaking. *Chem. Rev.* **2009**, *109*, 1346–1370.

(20) Tobias, D. J.; Stern, A. C.; Baer, M. D.; Levin, Y.; Mundy, C. J. Simulation and Theory of Ions at Atmospherically Relevant Aqueous Liquid-Air Interfaces. *Annu. Rev. Phys. Chem.* **2013**, *64*, 339–359.

(21) Pollard, T. P.; Beck, T. L. Toward a Quantitative Theory of Hofmeister Phenomena: From Quantum Effects to Thermodynamics. *Curr. Opin. Colloid Interface Sci.* **2016**, *23*, 110 – 118.

(22) Smith, D. E.; Dang, L. X. Computer simulations of NaCl association in polarizable water. *J. Chem. Phys.* **1994**, *100*, 3757–3766.

(23) Lamoureux, G.; Roux, B. Absolute Hydration Free Energy Scale for Alkali and Halide Ions Established from Simulations with a Polarizable Force Field. *J. Phys. Chem. B* **2006**, *110*, 3308–3322.

(24) Warshel, A.; Kato, M.; Pisliakov, A. V. Polarizable Force Fields: History, Test Cases, and Prospects. *J. Chem. Theory Comput.* **2007**, *3*, 2034–2045.

(25) Peng, T.; Chang, T.-M.; Sun, X.; Nguyen, A. V.; Dang, L. X. Development of Ions-TIP4P-Ew Force Fields for Molecular Processes in Bulk and at the Aqueous Interface Using Molecular Simulations. *J. Mol. Liq.* **2012**, *173*, 47–54.

(26) Shi, Y.; Xia, Z.; Zhang, J.; Best, R.; Wu, C.; Ponder, J. W.; Ren, P. Polarizable Atomic Multipole-Based AMOEBA Force Field for Proteins. *J. Chem. Theory Comput.* **2013**, *9*, 4046–4063.

(27) Kiss, P. T.; Baranyai, A. A New Polarizable Force Field for Alkali and Halide Ions. *J. Chem. Phys.* **2014**, *141*, 114501.

(28) Kohagen, Miriam and Pluhařová, Eva and Mason, Philip E. and Jungwirth, Pavel, Exploring Ion–Ion Interactions in Aqueous Solutions by a Combination of Molecular Dynamics and Neutron Scattering. *J. Phys. Chem. Lett.* **2015**, *6*, 1563–1567.

(29) Hassanali, A. A.; Cuny, J.; Verdolino, V.; Parrinello, M. Aqueous Solutions: State of the Art in Ab Initio Molecular Dynamics. *Phil. Trans. R. Soc. A* **2014**, *372*, 20120482.

(30) Wick, C. D.; Dang, L. X.; Jungwirth, P. Simulated Surface Potentials at the Vapor-Water Interface for the KCl Aqueous Electrolyte Solution. *J. Chem. Phys.* **2006**, *125*, 024706.

(31) Wick, C. D.; Kuo, I.-F. W.; Mundy, C. J.; Dang, L. X. The Effect of Polarizability for Understanding the Molecular Structure of Aqueous Interfaces. *J. Chem. Theory Comput.* **2007**, *3*, 2002–2010.

(32) Marenich, A. V.; Olson, R. M.; Chamberlin, A. C.; Cramer, C. J.; Truhlar, D. G. Polarization Effects in Aqueous and Nonaqueous Solutions. *J. Chem. Theory Comput.* **2007**, *3*, 2055–2067.

(33) Wick, C. D.; Xantheas, S. S. Computational Investigation of the First Solvation Shell Structure of Interfacial and Bulk Aqueous Chloride and Iodide Ions. *J. Phys. Chem. B* **2009**, *113*, 4141–4146.

(34) Wick, C. D. Electrostatic Dampening Dampens the Anion Propensity for the Air-Water Interface. *J. Chem. Phys.* **2009**, *131*, 084715.

(35) Guàrdia, E.; Skarmoutsos, I.; Masia, M. On Ion and Molecular Polarization of Halides in Water. *J. Chem. Theory Comput.* **2009**, *5*, 1449–1453.

(36) Yu, H.; Whitfield, T. W.; Harder, E.; Lamoureux, G.; Vorobyov, I.; Anisimov, V. M.; MacKerell, A. D.; Roux, B. Simulating Monovalent and Divalent Ions in Aqueous Solution Using a Drude Polarizable Force Field. *J. Chem. Theory Comput.* **2010**, *6*, 774–786.

(37) Caleman, C.; Hub, J. S.; van Maaren, P. J.; van der Spoel, D. Atomistic Simulation of Ion Solvation in Water Explains Surface Preference of Halides. *Proc. Natl. Acad. Sci. USA* **2011**, *108*, 6838–6842.

(38) Sun, L.; Li, X.; Tu, Y.; Agren, H. Origin of Ion Selectivity at the Air/Water Interface. *Phys. Chem. Chem. Phys.* **2015**, *17*, 4311–4318.

(39) Lisy, J. M. Spectroscopy and Structure of Solvated Alkali-Metal Ions. *Int. Rev. Phys. Chem.* **1997**, *16*, 267–289.

(40) Max, J.-J.; Chapados, C. IR Spectroscopy of Aqueous Alkali Halide Solutions: Pure Salt-Solvated Water Spectra and Hydration numbers. *J. Chem. Phys.* **2001**, *115*, 2664–2675.

(41) Miller, D. J.; Lisy, J. M. Hydrated Alkali-Metal Cations: Infrared Spectroscopy and ab Initio Calculations of $M^+(H_2O)_{x=25}Ar$ cluster ions for M = Li, Na, K, and Cs. *J. Am. Chem. Soc.* **2008**, *130*, 15381–15392.

(42) Heisler, I. A.; Meech, S. R. Low-Frequency Modes of Aqueous Alkali Halide Solutions: Glimpsing the Hydrogen Bonding Vibration. *Science* **2010**, *327*, 857–860.

(43) Gillan, M. J.; Alfè, D.; Michaelides, A. Perspective: How good is DFT for water? *J. Chem. Phys.* **2016**, *144*, 130901.

(44) Cisneros, G. A.; Wikfeldt, K. T.; Ojamäe, L.; Lu, J.; Xu, Y.; Torabifard, H.; Bartók, A. P.; Csányi, G.; Molinero, V.; Paesani, F. Modeling Molecular Interactions in Water: From Pairwise to Many-Body Potential Energy Functions. *Chem. Rev.* **2016**, *116*, 7501–7528.

(45) Bukowski, R.; Szalewicz, K.; Groenenboom, G. C.; van der Avoird, A. Predictions of the Properties of Water from First Principles. *Science* **2007**, *315*, 1249–1252.

(46) Bukowski, R.; Szalewicz, K.; Groenenboom, G. C.; van der Avoird, A. Polarizable Interaction Potential for Water from Coupled Cluster Calculations. I. Analysis of dimer potential energy surface. *J. Chem. Phys.* **2008**, *128*, 094313.

(47) Bukowski, R.; Szalewicz, K.; Groenenboom, G. C.; van der Avoird, A. Polarizable Interaction Potential for Water from Coupled Cluster Calculations. II. Applications to dimer spectra, virial coefficients, and simulations of liquid water. *J. Chem. Phys.* **2008**, *128*, 094314.

(48) Wang, Y.; Shepler, B. C.; Braams, B. J.; Bowman, J. M. Full-Dimensional, *Ab Initio* Potential Energy and Dipole Moment Surfaces for Water. *J. Chem. Phys.* **2009**, *131*, 054511.

(49) Wang, Y.; Huang, X.; Shepler, B. C.; Braams, B. J.; Bowman, J. M. Flexible, *Ab Initio* Potential, and Dipole Moment Surfaces for Water. I. Tests and Applications for Clusters up to the 22-mer. *J. Chem. Phys.* **2011**, *134*, 094509.

(50) Wang, Y.; Bowman, J. M. *Ab Initio* Potential and Dipole Moment Surfaces for Water. II. Local-Monomer Calculations of the Infrared Spectra of Water Clusters. *J. Chem. Phys.* **2011**, *134*, 154510.

(51) Babin, V.; Medders, G. R.; Paesani, F. Toward a Universal Water Model: First Principles Simulations from the Dimer to the Liquid Phase. *J. Phys. Chem. Lett.* **2012**, *3*, 3765–3769.

(52) Medders, G. R.; Babin, V.; Paesani, F. A Critical Assessment of Two-Body and Three-Body Interactions in Water. *J. Chem. Theory Comput.* **2013**, *9*, 1103–1114.

(53) Babin, V.; Paesani, F. The Curious Case of the Water Hexamer: Cage vs. Prism. *Chem. Phys. Lett.* **2013**, *580*, 1 – 8.

(54) Babin, V.; Medders, G. R.; Paesani, F. Development of a "First Principles" Water Potential with Flexible Monomers. II: Trimer Potential Energy Surface, Third Virial Coefficient, and Small Clusters. *J. Chem. Theory Comput.* **2014**, *10*, 1599–1607.

(55) Medders, G. R.; Babin, V.; Paesani, F. Development of a "First-Principles" Water Potential with Flexible Monomers. III. Liquid Phase Properties. *J. Chem. Theory Comput.* **2014**, *10*, 2906–2910.

(56) Hankins, D.; Moskowitz, J.; Stillinger, F. Water Molecule Interactions. *J. Chem. Phys.* **1970**, *53*, 4544–4554.

(57) Paesani, F. Getting the Right Answers for the Right Reasons: Toward Predictive Molecular Simulations of Water with Many-Body Potential Energy Functions. *Acc. Chem. Res.* **2016**, *49*, 1844–1851.

(58) Babin, V.; Leforestier, C.; Paesani, F. Development of a "First Principles" Water Potential with Flexible Monomers: Dimer Potential Energy Surface, VRT Spectrum, and Second Virial Coefficient. *J. Chem. Theory Comput.* **2013**, *9*, 5395–5403.

(59) Richardson, J. O.; Pérez, C.; Lobsiger, S.; Reid, A. A.; Temelso, B.; Shields, G. C.; Kisiel, Z.; Wales, D. J.; Pate, B. H.; Althorpe, S. C. Concerted hydrogen-bond breaking by quantum tunneling in the water hexamer prism. *Science* **2016**, *351*, 1310–1313.

(60) Cole, W. T. S.; Farrell, J. D.; Wales, D. J.; Saykally, R. J. Structure and Torsional Dynamics of the Water Octamer from THz Laser Spectroscopy Near 215 μm. *Science* **2016**, *352*, 1194–1197.

(61) Brown, S. E.; Götz, A. W.; Cheng, X.; Steele, R. P.; Mandelshtam, V. A.; Paesani, F. Monitoring Water Clusters "Melt" Through Vibrational Spectroscopy. *J. Am. Chem. Soc.* **2017**, *139*, 7082–7088.

(62) Reddy, S. K.; Straight, S. C.; Bajaj, P.; Huy Pham, C.; Riera, M.; Moberg, D. R.; Morales, M. A.; Knight, C.; Götz, A. W.; Paesani, F. On the Accuracy of the MB-pol Many-Body Potential for Water: Interaction Energies, Vibrational Frequencies, and Classical Thermodynamic and Dynamical Properties from Clusters to Liquid Water and Ice. *J. Chem. Phys.* **2016**, *145*, 194504.

(63) Pham, C. H.; Reddy, S. K.; Chen, K.; Knight, C.; Paesani, F. Many-Body Interactions in Ice. *J. Chem. Theory Comput.* **2017**, *13*, 1778–1784.

(64) Medders, G. R.; Paesani, F. Infrared and Raman Spectroscopy of Liquid Water through "First-Principles" Many-Body Molecular Dynamics. *J. Chem. Theory Comput.* **2015**, *11*, 1145–1154.

(65) Straight, S. C.; Paesani, F. Exploring Electrostatic Effects on the Hydrogen Bond Network of Liquid Water through Many-Body Molecular Dynamics. *J. Phys. Chem. B* **2016**, *120*, 8539.

(66) Reddy, S. K.; Moberg, D. R.; Straight, S. C.; Paesani, F. Temperature-Dependent Vibrational Spectra and Structure of Liquid Water from Classical and Quantum Simulations with the MB-pol Potential Energy Function. *J. Chem. Phys.* **2017**, *147*.

(67) Medders, G. R.; Paesani, F. Dissecting the Molecular Structure of the Air/Water Interface from Quantum Simulations of the Sum-Frequency Generation Spectrum. *J. Am. Chem. Soc.* **2016**, *138*, 3912–3919.

(68) Moberg, D. R.; Straight, S. C.; Knight, C.; Paesani, F. Molecular Origin of the Vibrational Structure of Ice Ih. *J. Phys. Chem. Lett.* **2017**, *8*, 2579–2583.

(69) Gaiduk, A. P.; Pham, T. A.; Govoni, M.; Paesani, F.; Galli, G. Electron Affinity of Liquid Water. *Nat. Commun.* **2018**, *9*, 247.

(70) Bajaj, P.; Götz, A. W.; Paesani, F. Toward Chemical Accuracy in the Description of Ion-Water Interactions Through Many-Body Representations. I. Halide-Water Dimer Potential Energy Surfaces. *J. Chem. Theory Comput.* **2016**, *12*, 2698–2705.

(71) Riera, M.; Mardirossian, N.; Bajaj, P.; Götz, A. W.; Paesani, F. Toward Chemical Accuracy in the Description of Ion–Water Interactions Through Many-Body Repre-

sentations. Alkali-Water Dimer Potential Energy Surfaces. *J. Chem. Phys.* **2017**, *147*, 161715.

(72) Bajaj, P.; Wang, X.-G.; Jr., T. C.; Paesani, F. Vibrational Spectra of Halide-Water Dimers: Insights on Ion Hydration from Full-Dimensional Quantum Calculations on Many-Body Potential Energy Surfaces. *J. Chem. Phys.* **2018**, *148*, 102321.

(73) Castleman, A.; Bowen, K. Clusters: Structure, Energetics, and Dynamics of Intermediate States of Matter. *J. Phys. Chem.* **1996**, *100*, 12911–12944.

(74) Duncan, M. A. Spectroscopy of Metal Ion Complexes: Gas-Phase Models for Solvation. *Annu. Rev. Phys. Chem.* **1997**, *48*, 69–93.

(75) Mahler, J.; Persson, I. A Study of the Hydration of the Alkali Metal Ions in Aqueous Solution. *Inorg. Chem.* **2011**, *51*, 425–438.

(76) Lee, S. H.; Rasaiah, J. C. Molecular Dynamics Simulation of Ion Mobility. 2. Alkali Metal and Halide Ions Using the SPC/E Model for Water at 25 C. *J. Phys. Chem.* **1996**, *100*, 1420–1425.

(77) Jensen, K. P.; Jorgensen, W. L. Halide, Ammonium, and Alkali Metal Ion Parameters for Modeling Aqueous Solutions. *J. Chem. Theory Comput.* **2006**, *2*, 1499–1509.

(78) Joung, I. S.; Cheatham III, T. E. Determination of Alkali and Halide Monovalent Ion Parameters for Use in Explicitly Solvated Biomolecular Simulations. *J. Phys. Chem. B* **2008**, *112*, 9020–9041.

(79) Varma, S.; Rempe, S. B. Coordination Numbers of Alkali Metal Ions in Aqueous Solutions. *Biophys. Chem.* **2006**, *124*, 192–199.

(80) Vaden, T. D.; Weinheimer, C. J.; Lisy, J. M. Evaporatively Cooled $M^+(H_2O)$ Ar Cluster Ions: Infrared Spectroscopy and Internal Energy Simulations. *J. Chem. Phys.* **2004**, *121*, 3102–3107.

(81) Vaden, T. D.; Lisy, J. M.; Carnegie, P. D.; Dinesh Pillai, E.; Duncan, M. A. Infrared Spectroscopy of the $Li^+(H_2O)Ar$ Complex: The Role of Internal Energy and Its Dependence on Ion preparation. *Phys. Chem. Chem. Phys.* **2006**, *8*, 3078–3082.

(82) Nicely, A. L.; Miller, D. J.; Lisy, J. M. Gas-Phase Vibrational Spectroscopy and Ab Initio Calculations of $Rb^+(H_2O)_n$ and $Rb^+(H_2O)_nAr$ Cluster Ions. *J. Mol. Spectros.* **2009**, *257*, 157–163.

(83) Schulz, F.; Hartke, B. Structural Information on Alkali Cation Microhydration Clusters from Infrared Spectra. *Phys. Chem. Chem. Phys.* **2003**, *5*, 5021–5030.

(84) Rajamani, S.; Ghosh, T.; Garde, S. Size Dependent Ion Hydration, Its Asymmetry, and Convergence to Macroscopic Behavior. *J. Chem. Phys.* **2004**, *120*, 4457–4466.

(85) Lee, H. M.; Tarakeshwar, P.; Park, J.; Kołaski, M. R.; Yoon, Y. J.; Yi, H.-B.; Kim, W. Y.; Kim, K. S. Insights into the Structures, Energetics, and Vibrations of Monovalent Cation-(Water) 1-6 Clusters. *J. Phys. Chem. A* **2004**, *108*, 2949–2958.

(86) Schulz, F.; Hartke, B. A New Proposal for the Reason of Magic Numbers in Alkali Cation Microhydration Clusters. *Theor. Chem. Acc.* **2005**, *114*, 357–379.

(87) Wang, Y.; Babin, V.; Bowman, J. M.; Paesani, F. The Water Hexamer: Cage, Prism, or Both. Full Dimensional Quantum Simulations Say Both. *J. Am. Chem. Soc.* **2012**, *134*, 11116–11119.

(88) Tuckerman, M. E. *Statistical Mechanics: Theory and Molecular Simulation*; Oxford University Press, 2010.

(89) Jensen, F. *Introduction to Computational Chemistry*; John Wiley & Sons, 2017.

(90) Cheng, X.; Steele, R. P. Efficient Anharmonic Vibrational Spectroscopy for Large Molecules Using Local-Mode Coordinates. *J. Chem. Phys.* **2014**, *141*, 104105.

(91) Cheng, X.; Talbot, J. J.; Steele, R. P. Tuning Vibrational Mode Localization with Frequency Windowing. *J. Chem. Phys* **2016**, *145*, 124112.

(92) Shimanouchi, T. *Tables of Molecular Vibrational Frequencies, Consolidated Volume I*, 1st ed.; National Bureau of Standards, 1972.

(93) Fraley, P. E.; Rao, K. N. High Resolution Infrared Spectra of Water Vapor: $\nu 1$ and $\nu 3$ Band of $H_2^{16}O$. *J. Mol. Spectros.* **1969**, *29*, 348–364.

(94) Partridge, H.; Schwenke, D. W. The Determination of an Accurate Isotope Dependent Potential Energy Surface for Water from Extensive Ab Initio Calculations and Experimental Data. *J. Chem. Phys.* **1997**, *106*, 4618–4639.

(95) Ke, H.; van der Linde, C.; Lisy, J. M. Insights into Gas-Phase Structural Conformers of Hydrated Rubidium and Cesium Cations, $M^+(H_2O)_n$ Ar (M= Rb, Cs; n= 3–5), Using Infrared Photodissociation Spectroscopy. *J. Phys. Chem. A* **2014**, *118*, 1363–1373.

(96) Towns, J.; Cockerill, T.; Dahan, M.; Foster, I.; Gaither, K.; Grimshaw, A.; Hazlewood, V.; Lathrop, S.; Lifka, D.; Peterson, G. D.; Roskies, R.; Scott, J. R.; Wilkins-Diehr, N. XSEDE: Accelerating Scientific Discovery. *Comput. Sci. Eng.* **2014**, *16*, 62–74.